

Engineering microfluidic papers: effect of fiber source and paper sheet properties on capillary-driven fluid flow

Alexander Böhm · Franz Carstens · Christian Trieb · Samuel Schabel · Markus Biesalski

Received: 18 July 2013 / Accepted: 23 December 2013 / Published online: 4 January 2014
© Springer-Verlag Berlin Heidelberg 2014

Abstract In the present study, we introduce a novel approach to control and modulate fluid transport inside microfluidic papers using lab-engineered paper sheets. Lab-sheets consisting of different fiber sources (eucalyptus sulfate and cotton linters pulp) and varying porosities were designed and further modified with small millimeter-scaled channels using hydrophobic barriers consisting of fiber-attached, hydrophobic polymers. The capillary-driven transport of an aqueous solution was monitored visually, and the influence of parameters such as fiber source, paper grammage, and channel width on the flow rates through the channel was investigated. The experimental results were compared with those obtained with commercially available filter papers. Our findings suggest that accurate control of fluid transport processes with standard filter papers is complex. Additionally, if the channel width is smaller than the mean fiber length, flow rates become dependent on the geometric parameters of the channel because of the formation of dead-end pores at the hydrophobic barriers.

Electronic supplementary material The online version of this article (doi:10.1007/s10404-013-1324-4) contains supplementary material, which is available to authorized users.

A. Böhm · M. Biesalski (✉)
Laboratory of Macromolecular Chemistry and Paper Chemistry,
Department of Chemistry, Technische Universität Darmstadt,
64287 Darmstadt, Germany
e-mail: biesalski@tu-darmstadt.de

A. Böhm · M. Biesalski
Center of Smart Interfaces (CSI), Technische Universität
Darmstadt, 64287 Darmstadt, Germany

F. Carstens · C. Trieb · S. Schabel
Laboratory of Paper Technology, Department of Mechanical
Engineering, Technische Universität Darmstadt,
64283 Darmstadt, Germany

Finally, control of the paper sheets porosity, by varying the fiber density of the lab-made paper, affords the fabrication of chemically identical sheets whereby capillary flow is largely influenced and can be modulated accordingly by simple papermaking processes.

Keywords Paper microfluidics · Low-cost · Point-of-care diagnostics · Fluid transport

1 Introduction

In recent years, paper-based microfluidic devices have gained increasing interest for the development of low-cost point-of-care diagnostic tools (Martinez et al. 2010; Li et al. 2012; Cheng et al. 2010; Songjaroen et al. 2012; Phillips and Lewis 2013). The use of paper as a substrate for microfluidic applications is highly attractive because of numerous advantages: (1) Unlike conventional microfluidic platforms, no external pumps are required for fluid transport inside the paper because of capillary forces; (2) paper consists of cellulose, a renewable and very cheap material; and (3) the surface of the cellulose fibers can be modified with different chemical functions for the definition of hydrophobic barriers (i.e., small channels inside the paper sheets), or conjugated with sensing elements (i.e., immobilization). To realize spatial control of aqueous fluids inside a paper substrate, hydrophobic barriers have been designed inside paper substrates by various means that include physical blockage of the pores using photoresists (Martinez et al. 2007, 2008; Klasner et al. 2010), polydimethylsiloxane (PDMS) polymers (Bruzewicz et al. 2008), and wax (Lu et al. 2009; Carrilho et al. 2009; Leung et al. 2010). Other approaches include chemical hydrophobization of the cellulose fiber surface using small

reactive molecules, such as alkyl ketene dimers (AKD), which can thermally bind to the hydroxyl groups of the cellulosic fibers (Li et al. 2008, 2010), and hydrophobic polymers that can be linked to the organic paper matrix by ultraviolet (UV) irradiation (Böhm et al. 2013a, b). Besides the development of simple diagnostic tools, food quality control devices, and other low-cost analytical tools, understanding and controlling the lateral flow of a (complex) fluid within a paper channel may lead to further applications of paper-based micro-engineering devices, ranging from paper-based micromixers and reactors (Liana et al. 2012; Fu et al. 2010a) to functional paper for regenerative medicine. Fu et al. showed that the flow rate of a fluid within a paper strip of constant width and varying length is dependent on the resistance developed by the wet paper behind the fluid front (Fu et al. 2010a, b). Fluid transport follows a $t^{1/2}$ dependency and therefore can be described by a simple Lucas–Washburn model for static viscous flows, as demonstrated by researchers (e.g., Hodgson and Berg 1988). Another group more recently showed that by changing the width of the paper channel, similar control of the fluid transport can be attained. Dissolvable barriers can also be used as flow modulators, which can delay the movement of a fluid in specific segments of the paper network (Fu et al. 2010b). In other studies, Phillips and coworkers developed 3D paper-based fluidic timers that were based on non-dissolvable blocking patches (Phillips and Lewis 2013; Noh and Phillips 2010a, b). Varying quantities of paraffin wax were applied to alter the wetting properties of the paper in a controlled fashion.

Although considerable progress has been made in the design of such fluidic timers using paper-based substrates, to date, all strategies have been based on the use of simple commercially available filter papers. However, fluid transport in an engineered paper sheet does not exclusively rely on the geometric definition of the channel itself, but is strongly dependent on the intrinsic parameters of the cellulosic material such as the type of fiber used during paper fabrication, length and diameter of the fibers, swelling properties of the fibers in an aqueous environment, orientation of the paper fibers, and the number of fibers per unit volume of the paper sheet (i.e., the density of the sheet). Thus, it is of great interest to understand the influence of such parameters on the fluid transport in microfluidic papers. Understanding fluid transport behaviors based on simple paper engineering processes and using papers of varying compositions, morphologies, and topologies are of particular interest.

In this paper, we introduce the use of lab-engineered paper substrates for controlling fluid transport within paper-defined channels. Conventional papermaking laboratory instruments and varying fiber sources (eucalyptus sulfate and cotton linters pulp) were used for the fabrication process. The pore sizes (i.e., porosity) of the lab-sheets

were adjusted by controlling the fiber density of the lab-engineered papers. In addition, small millimeter-scaled channels were designed by photochemical attachment of barriers consisting of hydrophobic polymers, which were covalently bound to the cellulosic fibers of the preformed paper sheets. Capillary-driven fluid transport of an aqueous solution inside the paper-defined channels was monitored on a video camera. We show that by adjusting the fiber density of the paper sheets that influences the pore sizes and porosities of the lab-sheets in the papermaking process, it is possible to modulate the fluid transport process in such microfluidic papers. Additionally, we demonstrate that the influence of the channel width and fiber length is critical, and that fluid transport becomes independent of the channel width when the latter exceeds the length of the fibers used in the isotropically layered fiber sheets. Finally, comparison studies with commercially available filter paper grades show that direct extraction of quantitative information for successful design of fluid timer settings is complex as various paper grades yield different results though similar paper grammages are being compared.

2 Experimental

2.1 Materials

2,2'-Azobis(2-methylpropionitrile) (AIBN, >98 %, Fluka), 4-hydroxybenzophenone (98 %, Alfa Aesar), fluorescein (>98 %, Merck), triethylamine (99 %, Grüssing GmbH), cyclohexane (p.a., Biesterfeld), dichloromethane (p.a., Biesterfeld), dimethyl sulfoxide (DMSO, 99 %, Grüssing GmbH), ethyl acetate (p.a., Biesterfeld), methanol (>99.5 %, BASF), tetrahydrofuran (THF, >99.5 %, Roth), 1,4-dioxane (>99.5 %, Roth), Roth Rotilabo 15A filter paper (Roth 15A, grammage: 84 g m⁻²; Brunauer–Emmett–Teller surface area: 1.2 m² g⁻¹; mean pore radius: 2.3 μm), Whatman No. 1 filter paper (grammage: 88 g m⁻²; mean pore radius: 5.4 μm), and pulp (fiber source: cotton linters (curl: 17.4 %; fibrillation degree: 4.9 %; fines content: 6.5 %; lignin content: <1 %) and eucalyptus sulfate (curl: 15.7 %; fibrillation degree: 4.7 %; fines content: 1.5 %; lignin content: <1 %) were used as received. Methyl methacrylate (MMA, 99 %, Sigma-Aldrich) and methacryloyl chloride (97 %, Sigma-Aldrich) were flowed through a basic alumina column, distilled under reduced pressure, and stored under nitrogen prior to use.

2.2 Monomer and polymer synthesis

The synthesis of the photoreactive monomer 4-methacryloyloxybenzophenone (MABP) was carried out according to protocols by Berchtold (Berchtold 2005) and Freidank

(Freidank 2005). The fluorescent monomer fluorescein-*O*-methacrylate (FOMA) was synthesized according to the procedure described by Berchtold (Berchtold 2005); details of the synthesis can be obtained in a recent publication (Böhm et al. 2013a). All polymers described below were prepared by free-radical copolymerization and characterized with respect to molar mass and composition by size exclusion chromatography (PSS SDV linear M was used as column, THF as eluent, and the system was calibrated using narrow dispersed polystyrene standards) and ^1H NMR spectroscopy, respectively. The detailed synthesis of the photoreactive fluorescent P(MMA-*co*-MABP-*co*-FOMA) has been reported in a recent publication (Böhm et al. 2013a).

2.2.1 P(MMA-*co*-MABP)

Methyl methacrylate (4.2 mL, 39.0 mmol) was added to 4-methacryloyloxybenzophenone (266.0 mg, 1.0 mmol) in 1,4-dioxane (25 mL) in a Schlenk flask under a nitrogen atmosphere. The initiator AIBN (19.4 mg, 0.12 mmol) was added, and the solution was degassed using four freeze-pump-thaw cycles. The flask was placed in a thermostated bath at 60 °C for 16 h for polymerization. The polymer was then precipitated in methanol (350 mL) and dried under vacuum. The polymer was purified by re-precipitation with THF (15 mL) and methanol (200 mL). The polymer was obtained as a white solid (1.6 g, 36 %), $M_n = 49,000 \text{ g mol}^{-1}$. ^1H NMR analysis yielded a molar composition of $\sim 3.5 \text{ mol } \%$ of the photoreactive benzophenone group in the copolymer.

2.3 Preparation of lab-engineered paper sheets

For the preparation of lab-engineered paper substrates, bleached, dry cotton linters, and eucalyptus sulfate pulp were used. The pulp was refined in a Voith LR 40 laboratory refiner. After the refining process, the cotton linters pulp and eucalyptus sulfate pulp had Schopper-Riegler ($^{\circ}\text{SR}$) values of 37 and 18, respectively. Refining was performed with an effective specific energy of 200 kWh t^{-1} (cotton linters) and 16 kWh t^{-1} (eucalyptus). For the cotton linters pulp-based lab-engineered paper sheets, a series of paper sheets, consisting of isotropically layered cellulose fibers, with grammages of 23.5 ± 0.3 , 45.5 ± 1.0 , 76.4 ± 0.6 , and $161 \pm 0.5 \text{ g m}^{-2}$ was fabricated on a conventional Rapid-Koethen hand sheet maker according to DIN 54358 and ISO 5269/2 in the absence of additives and fillers. For the eucalyptus sulfate pulp-based lab-engineered paper sheets, paper sheets, consisting of isotropically layered cellulose fibers with a grammage of $94.9 \pm 0.6 \text{ g m}^{-2}$, were fabricated by the same above-mentioned process.

After sheet formation, paper substrates were equilibrated at 23 °C and 50 % relative humidity (climate room condition) for at least 24 h before further characterization was performed. At this point, the paper sheets on average contain about 6 % water, taken up from the humid air. All paper sheet characterizations (Sect. 2.5) were performed at a constant temperature and relative humidity (23 °C and 50 % relative humidity).

2.4 Preparation of paper-defined channels

For the preparation of the paper-defined channels, the paper substrates were cut into pieces ($2.5 \times 7.5 \text{ cm}$). P(MMA-*co*-MABP) and P(MMA-*co*-MABP-*co*-FOMA) copolymers were first dissolved in THF at a concentration of $\sim 30 \text{ mg mL}^{-1}$. The functional polymers were adsorbed onto the paper by submerging the paper substrates into the polymer solution for ca. 20 s (dip-coating method) followed by subsequent air-drying for ca. 30 min. After the polymers were adsorbed onto the cellulose fibers of the paper sheets, the samples were transferred to a Vilber Lourmat Bio-Link BLX UV exposure chamber and irradiated with UV light ($\lambda = 254 \text{ nm}$). All samples were illuminated with a energy of 400 mJ cm^{-2} , $\sim 94 \%$ of the benzophenone groups reacted (Berchtold 2005). This energy dose corresponds to an illumination time of $\sim 16 \text{ min}$. To prepare the polymer-defined channels, appropriate metal masks were contacted with the paper substrate during the illumination step. All prepared channels had a width of 4 mm, unless stated otherwise.

The lab-engineered paper sheets that comprised the model filter papers (Roth 15A, thickness: 140 μm ; and Whatman No. 1, thickness: 180 μm) and featured grammages of 76 g m^{-2} (cotton linters, thickness: 162 μm), 95 g m^{-2} (eucalyptus sulfate, thickness: 180 μm), and 161 g m^{-2} (cotton linters, thickness: 291 μm) necessitate illumination on both sides of the substrate to ensure homogenous immobilization of the functional polymers throughout the entire thickness of the paper substrate [further details can be obtained in a recent publication (Böhm et al. 2013a)]. Following illumination, the non-bound polymer was removed from the shaded areas by solvent extraction for 150 min that was conducted in a Soxhlet apparatus using THF as the solvent. All samples were air-dried for at least 15 h prior to use.

2.5 Characterization of lab-engineered and polymer-modified paper substrates

Fluorescent micrographs were captured on an Olympus BX60 fluorescent microscope equipped with an Olympus XM10 camera. Image analysis was performed using ImageJ software. Video streams were recorded on a Panasonic

SDR-S150 video camera. The video streams were analyzed using MPEG Streamclip and Corel Draw. The mean pore radii and porosities were determined by mercury porosimetry using a Micromeritics AutoPore IV 9500 (all measurements were performed in duplicate, and typical data obtained by mercury porosimetry (cumulative pore volume, pore size distribution) are shown in Figure S2). The thickness of the lab-engineered paper sheets was analyzed on a Karl Schröder KG 200-A. The fiber length of the cotton linters pulp was determined via optical microscopy using a Zeiss Stemi 2000-C microscope. Grammages of the prepared lab-sheets were calculated using Eq. 1 according to DIN EN ISO 536:

$$\text{Grammage} = \frac{hm_{\text{dry}}}{A} \times 10^6, \quad (1)$$

where $h = 1.07$ is an empirical constant accounting for water-uptake of the sheets at a constant relative humidity of 50 % (see Sect. 2.3 for details), m_{dry} (g) is the mass of the dried paper sheet, and A (mm^2) is the surface area of the used lab-sheet.

2.6 Analysis of fluid transport inside paper-defined channels

To study the fluid transport through the paper-defined channels, the paper substrates were clamped between two PMMA slides and the inlets of the Y channel were connected to syringe pumps via silicon tubes (inner diameter: 2 mm). The syringe pumps were used to transport aqueous solutions to the channel inlet through the silicon tubes. When the liquid front reached the channel inlet, pressure on the syringe pumps was set to zero, and the liquid entered the channels via capillary forces. To prevent pressure differences between the silicon pipes and the paper channel, the syringe pumps were positioned at the same height as the microfluidic papers. Fluid transport through the paper-defined channels was investigated in situ via video streaming, and the individual data points of the 1D position of the fluid front at a given time were investigated after video capture. To investigate the reproducibility of the separate experiments performed with similar paper channels, the fluid transport through five paper-defined channels, based on the same paper substrate (eucalyptus sulfate, 95 g m^{-2}), was examined by analyzing the linear distance, x , as a function of $t^{0.5}$ for each prepared channel. The mean values of $x(t)$ with the associated standard deviations can be found in Figure S1.

3 Results and discussion

First, we investigated the influence of paper porosity and the type of pulp fibers used in paper preparation on fluid

transport inside small channels of paper substrates. Both commercially available filter papers and the various lab-engineered paper substrates were of interest. The commercially available filter papers and the lab-sheets prepared herein were subjected to chemical modification via a photolithographic approach, using photoreactive polymers, to design small double-Y channels in the respective paper substrates, as shown in Fig. 1.

The commercial filter papers were compared with our lab-engineered paper sheets. Roth 15A and Whatman No. 1, which are both extensively used by many researchers for designing microfluidic paper devices, were used as model filter papers. All papers were characterized in terms of average pore size, grammage, and thickness using methods, as outlined in the Experimental section, prior to use in the fluidic experiments. The properties of the paper substrates used in the first series of experiments are presented in Table 1.

The fluid transport within the paper-defined channels was examined; the substrate was clamped between two PMMA slides, and the inlets of the Y channel were connected to fluid reservoirs via silicon tubes (Fig. 2a, b). The aqueous solutions were introduced through the channels by capillary forces action following initial pumping. The capillary-driven transport of the fluid through the paper-defined channels was observed in situ via video streaming, and the individual data points of the 1D position of the fluid front after a given time were analyzed after video capture (Fig. 2c).

The profile of the flow was fitted according to the Washburn model (Eq. 2), which describes a static viscous flow (Lucas 1918; Washburn 1921). The nonlinearized (x as a function of t) and linearized profiles (x as a function of $t^{0.5}$) are shown in Fig. 3b, c, respectively.

$$x(t) = \sqrt{\frac{\sigma t r \cos \theta}{2\eta}} \quad (2)$$

Here, x is the distance moved by the fluid front, σ is the surface tension, t is the time, r is the average pore radius determined by mercury porosimetry, θ is the contact angle, and η is the viscosity.

As observed in Fig. 3c, a linear relationship was obtained for all the studied paper substrates and corresponds to the expected Washburn-type flow as described by Eq. 2. These results indicate the presence of a strictly capillary-driven viscous flow inside the paper channels. Interestingly, the model filter paper Roth 15A exhibits a significantly smaller slope relative to those of the Whatman No. 1 filter paper and cotton linters-based lab-engineered paper substrate though all papers featured similar paper grammages. However, a slower fluid transport is expected for the Roth 15A filter paper, based on the Lucas–Washburn kinetics model, because of its smaller pore size when compared with that of the other paper substrates (Table 1). In contrast, Whatman

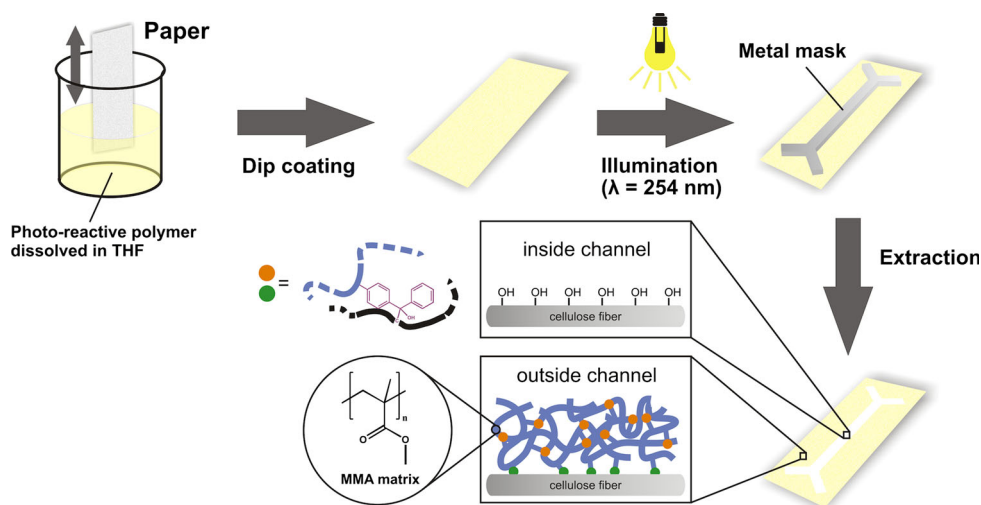


Fig. 1 Schematic illustration of the process employed to create the polymer-defined channels inside paper substrates. Photoreactive polymers are first adsorbed onto the cellulose fibers using the dip-coating method. During illumination with UV light, a channel-defining metal mask is brought into contact with the paper substrate; a surface-attached polymer network is formed in the non-shaded area through a photochemical reaction between the benzophenone group

and the aliphatic C–H groups of the cellulose fibers (*green dots*) and other polymer segments in close proximity (*orange dots*) (for details of the photochemical reaction, see Böhm et al. 2013a, b). Development of the chemical micro-pattern is achieved following removal of non-bound macromolecules in shaded areas via solvent extraction (color figure online)

Table 1 Properties of the paper substrates

Paper substrate	Pore radius (μm)	Grammage (g m ⁻²)	Thickness (μm)	Porosity
Roth 15A	2.3	84	140	0.60
Eucalyptus sulfate	4.2	95	180	0.65
Cotton linters	4.3	76	160	0.69
Whatman No. 1	5.4	88	180	0.66

No. 1 filter paper and cotton linters-based lab-engineered paper sheets displayed significantly steeper slopes (Fig. 3c). Although this finding may be explained by their larger pore size properties (Table 1), the influence of other parameters, such as surface chemistry of the fiber source and morphology of the fiber surface, needs to be considered. In particular, in the case of commercially available filter papers, additional aspects that can potentially influence fluid transport kinetics need to be accounted for. For instance, filter papers usually comprise cross-linked polymers that serve as wet-strengthening additives; these cannot be removed by solvent extraction. Thus, these polymers could potentially influence fluid transport behaviors inside paper-defined channels.

In addition to the lab-sheets fabricated from cotton linters, we prepared paper sheets from eucalyptus sulfate pulp. As shown in Fig. 3, the transport of an aqueous solution inside eucalyptus pulp-based paper substrates is faster when compared with that in cotton linters-based papers of comparable pore radii (Table 1). Relative to the cotton linters pulp, the eucalyptus sulfate pulp may contain charged lignin residues as well as hemicelluloses. As

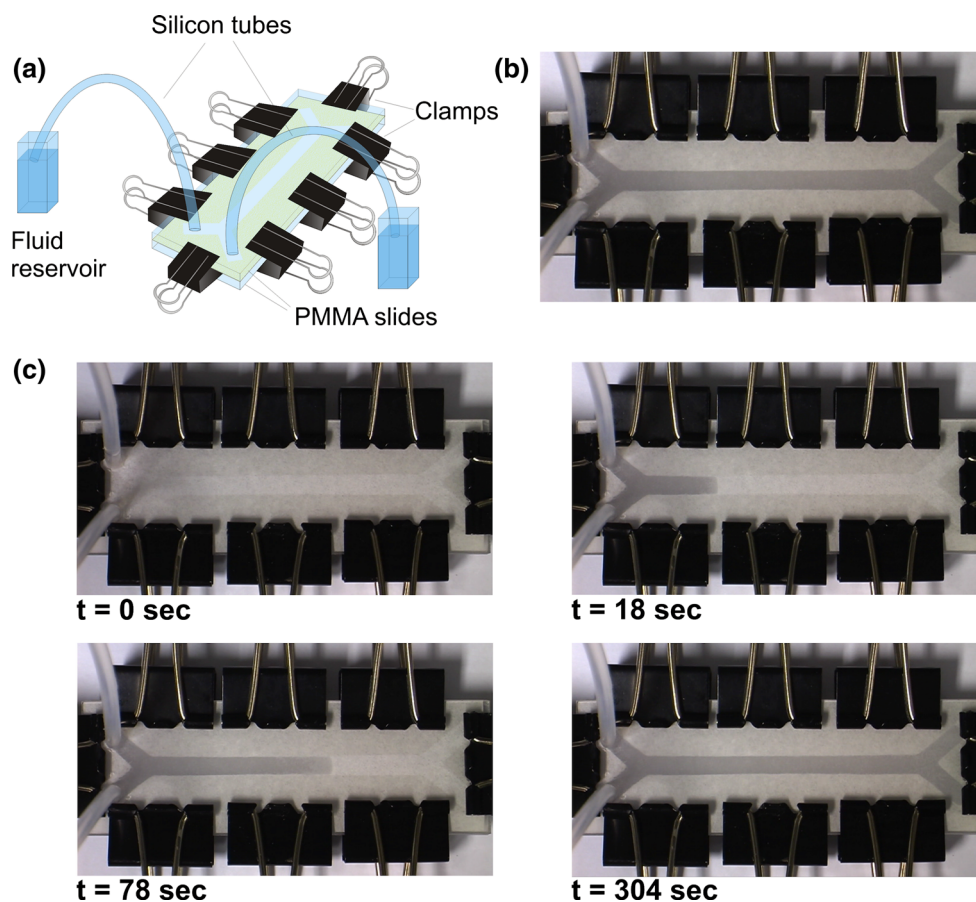
H₂SO₄ and NaOH are used during the pulping process of eucalyptus, the lignin residues on the eucalyptus fiber surface may contain SO₃⁻H⁺ and SO₃⁻Na⁺ groups (lignin sulfonates). Differences in the fiber surface chemistry may therefore be responsible for differences in transport kinetics when different paper sheets are compared.

The time taken for the fluid to travel along the straight 50-mm channel for the different studied paper substrates is as follows: 18 min (Roth 15A); 16 min 30 s (lab-engineered cotton linters-based paper, 76 g m⁻²); 8 min 30 s (Whatman No. 1); and 6 min 10 s (lab-engineered eucalyptus sulfate-based paper, 95 g m⁻²). The different fluid transport kinetics observed for the various paper substrates, as indicated by changes in the slope (Fig. 3c), can be further described by calculating flow rates for the fluid transport inside the paper-defined channels. As mentioned earlier, the 1D transport of the fluid front within the channels can be described by a simple Washburn model that accounts for a wet-out flow regime in a porous medium (Kauffman et al. 2010). As inferred from Eq. 2, the square of the distance, *x*², is proportional to the time *t*. Thus, with increasing time (i.e., distance), the rate of flow through a porous channel constantly changes, and comparison of average flow rates is only valid within a given time interval (i.e., distance). The average flow rates were calculated as follows:

$$v_c = \frac{V_{\text{free}}}{t} \quad \text{with } V_{\text{free}} = V_{\Sigma}p, \tag{3}$$

where *v_c* is the average flow rate; *V_{free}* is the free pore volume; *V_Σ* is the total volume of the channel segments, as

Fig. 2 **a** Schematic representation of the assembled paper device. The paper substrate containing the channel was clamped between two PMMA slides, and the inlets of the Y channel were brought into contact with two fluid reservoirs containing distilled water. **b** Photograph of a fluid-containing paper-defined channel based on a lab-engineered paper substrate (cotton linters, grammage: 23 g m^{-2}). **c** Image sequence of fluid flow inside the paper-defined channel; images were captured at 0, 18, 78, and 304 s after the fluid was brought into contact with the channel



defined by the length and the width of the channel, and the thickness of the paper substrate; t is the time; and p is the porosity of the paper substrate. Comparison of the apparent flow rates was made by analyzing the flow at the channel inlet (i.e., first 10 mm) and the flow at the end of the channel (i.e., last 10 mm). The calculated v_c values are given in Table 2. As inferred from Table 2, the average flow rates near the channel inlet vary over a wide range from $\sim 2.5 \mu\text{L min}^{-1}$ (Roth 15A) to $\sim 11 \mu\text{L min}^{-1}$ (eucalyptus-based paper substrates), and those near the channel outlet vary between $\sim 0.6 \mu\text{L min}^{-1}$ (Roth 15A) and $\sim 2.3 \mu\text{L min}^{-1}$ (eucalyptus-based paper substrates). The apparent Reynolds number was calculated using the apparent flow rate, as follows:

$$\text{Re} = \frac{\rho v d}{\eta} = \frac{v d}{\nu} \quad \text{with } \eta = \nu \rho, \quad (4)$$

where ρ (kg m^{-3}) is the density of the fluid, v (m s^{-1}) is the average flow velocity, d (m) is the length, ν ($\text{m}^2 \text{s}^{-1}$) is the kinematic viscosity of the fluid, and η ($\text{kg m}^{-1} \text{s}^{-1}$) is the dynamic viscosity of the fluid. A density of $\rho = 998 \text{ kg m}^{-3}$, a kinematic viscosity of $\nu = 10^{-6} \text{ m}^2 \text{s}^{-1}$, and a dynamic viscosity of $\eta = 0.001 \text{ kg m}^{-1} \text{s}^{-1}$ were used for Reynolds number calculations to describe the microfluidic papers.

Laminar flows are typically observed for common flow velocities when a particular dimension of the device is smaller than 1 mm (Osborn et al. 2010; Brody et al. 1996; Prucell 1977). Hence, laminar flow would be expected for paper-based microfluidic platforms as the characteristic length of a paper substrate is equivalent to the mean pore diameter, which is $\ll 1$ mm, thereby resulting in very low Reynolds numbers, in the order of $\sim 10^{-3}$, as discussed in detail by Osborn et al. (2010). The calculated Reynolds numbers for the microfluidic papers investigated in the present study are shown in Table S1, and they are all in the order of $\sim 10^{-3}$, confirming the development of a laminar flow inside the individual pores of the paper-defined channels.

Fu et al. (2010b) investigated the transport of an aqueous fluid inside paper-defined channels of varying widths. An increase in the speed of fluid transport was observed at decreasing channel width. This trend was explained by the fact that with increasing volume (i.e., width) of the paper channel, the fluid needs more time to penetrate into the corresponding porous system. The smallest dimension (length) of the paper segments used in the latter experiment was 3 mm. In contrast, we used cellulose microfibrils that were up to 3 mm in length. A series of cotton linters lab-sheets with varying channel widths and a grammage of

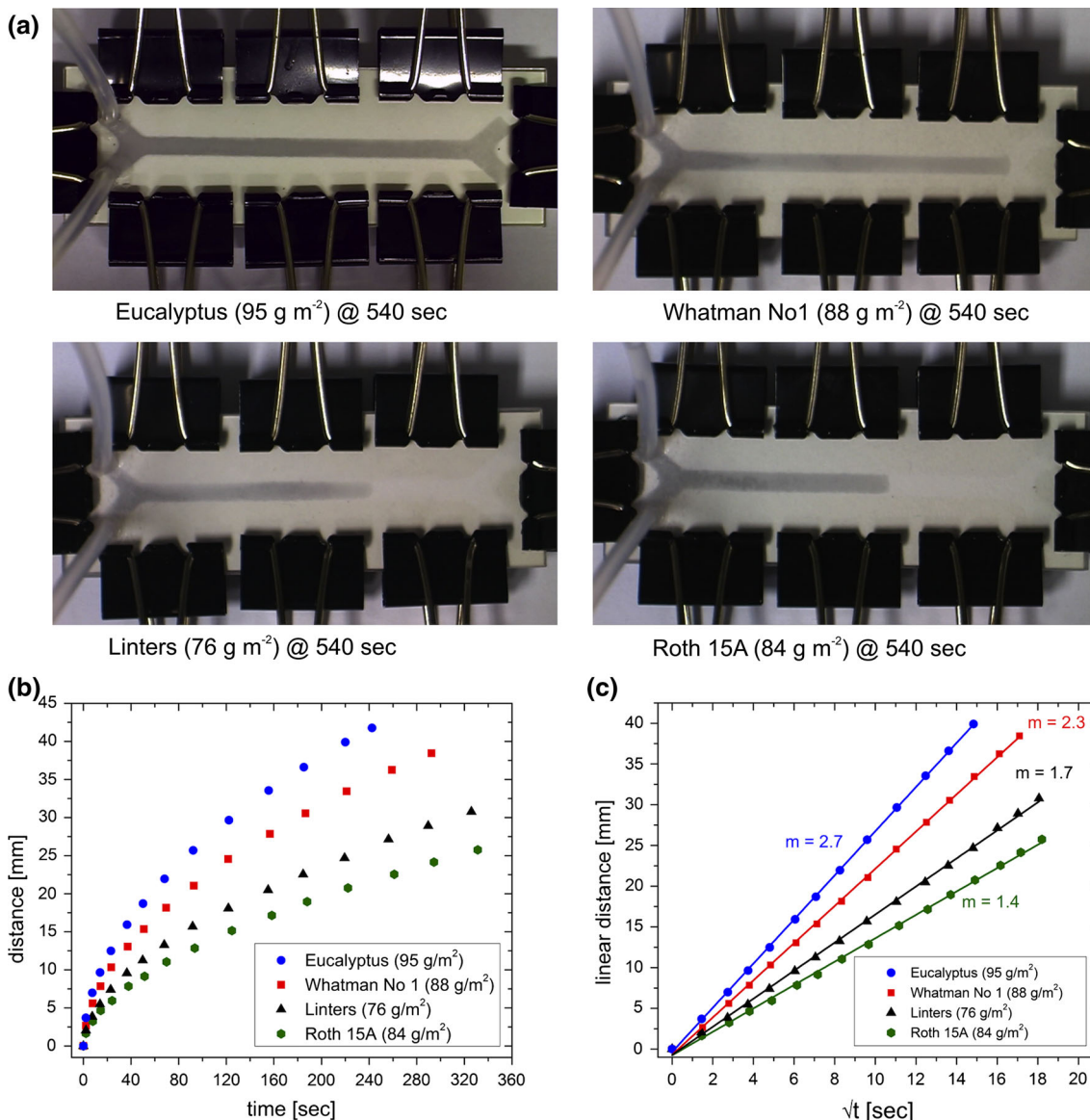


Fig. 3 **a** Comparison of the 1D position of the fluid front inside the paper-defined channels for different paper substrates at a given time interval. Photographs were taken at ~9 min after the fluid was brought into contact with the channels. **b** Comparison of the 1D position, x , of the fluid front driven by capillary action along the channel as a function of time for the investigated paper substrates. Individual data points were captured by video streaming the capillary transport of the fluid inside the channel. The expected relationship

between distance, x , and time was observed for all paper substrates; that is, the further the distance of the fluid front from the channel inlet, the longer the time taken by the fluid front to move a certain distance inside the channel. By using different paper sources, the distance covered by the fluid front within a given time interval can be controlled over a wide range. **c** Comparison of the 1D position, x , of the fluid front driven by capillary action along the channel as a function of $t^{0.5}$ for the investigated paper substrates

23 g m⁻² was prepared herein. All substrates were prepared by UV photolithography using masks of different sizes, as described in the Experimental section. Observation of the channels and determination of the channel dimensions were assisted with fluorescently labeled PMMA polymers that were used to define the hydrophobic barriers. Figure 4 shows fluorescent images of the channels with varying width (1–5 mm).

The paper substrates containing the channels of varying widths were clamped between two PMMA slides, and the inlets of the Y channel were connected to fluid reservoirs via silicon tubes. The capillary-driven transport of the fluid front inside the paper-defined channels was observed by video streaming, as described earlier, and the individual data points were plotted as a function of t (Fig. 5a) and $t^{0.5}$ (Fig. 5b) according to the Lucas–Washburn kinetics model.

Table 2 Apparent flow rates for the paper substrates

Paper substrate	Pore radius (μm)	V_{free} (μL)	v_c ($\mu\text{L min}^{-1}$)
Roth 15A	2.3	16.8	2.5 ± 0.25 – 0.6 ± 0.06
Whatman No. 1	5.4	23.8	8.6 ± 0.80 – 1.6 ± 0.16
Cotton linters	4.3	22.4	3.7 ± 0.36 – 0.8 ± 0.07
Eucalyptus sulfate	4.2	23.4	11.2 ± 1.2 – 2.3 ± 0.19

As observed from Fig. 5b, the capillary-driven fluid flow inside the channels can be described as a Washburn-type viscous flow. Interestingly, significant differences in the slope were observed for the different channel dimensions. For the channels having a width between 2 and 5 mm, a steeper slope from 3.5 to 4.4 was observed as the channel width decreased from 5 to 2 mm. Faster flows are expected in narrow channels as they exhibit smaller free pore volumes. The observed trend is consistent with the findings by Yager and coworkers (Fu et al. 2010b). However, analysis of the paper substrate with the smallest channel width (i.e., 1 mm) revealed an unexpected small slope of 3.3. Comparisons based on absolute time scales revealed the following: Travelling time of the fluid along the straight part of the channel in the 1-mm channel is about 4 min 20 s, whereas that in the 2-mm channel is about 2 min 20 s. To understand these findings on a quantitative basis, the average flow rates at channel segments (i.e., channel inlet and outlet) were calculated according to Eq. 3, and the results are presented in Table 3.

As inferred from Table 3, the average flow rates near the channel inlet vary over a wide range from $\sim 2.3 \mu\text{L min}^{-1}$ (channel width: 1 mm) to $\sim 15.5 \mu\text{L min}^{-1}$ (channel width: 4 and 5 mm), and those near the channel outlet range between $\sim 0.4 \mu\text{L min}^{-1}$ (channel width: 1 mm) and $\sim 2.4 \mu\text{L min}^{-1}$ (channel width: 4 and 5 mm). Flow rates were similar at channel widths above 4 mm. The flow rates significantly decreased with decreasing channel width; this trend is contrary to the findings by Fu et al. (2010b).

The different trend obtained herein was likely influenced by the fiber length in the isotropically layered cellulosic microfibrils inside the paper sheets. The fiber length of the cotton linters pulp used for the preparation of the lab-sheets varies between 2 and 3 mm (as statistically analyzed by optical microscopy). For microfluidic papers with channel width of 1–3 mm, which is comparable to the fiber length itself, we can expect a large amount of pores that are “terminated” at the channel walls (dead-end pores), i.e., PMMA-defined hydrophobic barrier. The flow of fluid that encounters such dead-end pores is interrupted because of the hydrophobic barrier. As a result, a fluid front that encounters dead-end pores requires longer apparent time to fill a given volume of defined space with a certain length when compared with a fluid that flows through pores that are not terminated, e.g., a channel wall. Thus, an increasing number of dead-end pores may result in an “apparent decrease of the pore diameter” of the remaining accessible pores, thereby leading to a decrease in the apparent porosity of the paper sheet. As shown earlier, smaller pore radii can lead to a decrease in the apparent flow rates within paper-defined channels.

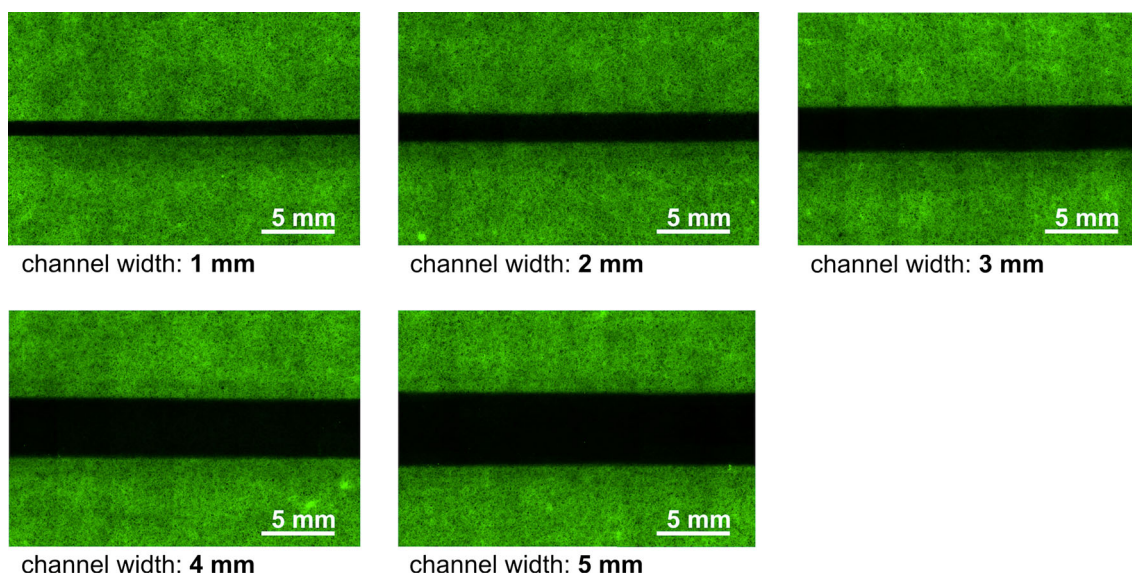


Fig. 4 Fluorescent images of P(MMA-co-MABP-co-FOMA)-modified paper substrates following illumination through channel-defining masks featuring widths between 1 and 5 mm. For a comprehensive

view of the micro-structured surface, numerous images of the same substrate were collated and presented

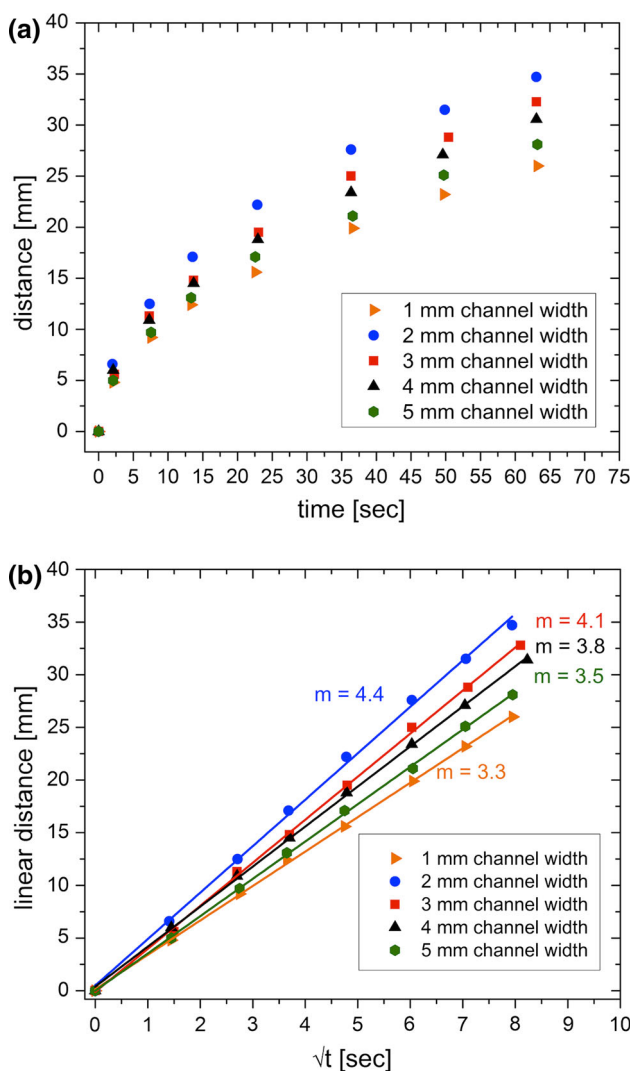


Fig. 5 **a** Comparison of the 1D position, x , of the fluid front driven by capillary action along the channel as a function of time for the paper-defined channels with different widths. Individual data points were captured by video streaming the capillary transport of the fluid inside the channel. The expected relationship between distance, x , and time was observed for all the studied channel widths; that is, the further the distance of the fluid front from the channel inlet, the longer the time taken for the fluid front to move a certain distance inside the channel. By varying the width of the channel, the distance covered by the fluid front within a given time interval can be controlled over a wide range. **b** Comparison of the 1D position, x , of the fluid front driven by capillary action along the channel as a function of $t^{0.5}$ for the paper-defined channels with different widths

Finally, the influence of the porosity of the paper substrate (i.e., free pore volume in a given channel) on fluid transport was investigated. A series of cotton linters-based paper sheets with different fiber densities was prepared as outlined in the Experimental section. Because all papers investigated in this set of experiments were prepared from the same fiber type, resulting changes in fluid dynamics based on fiber length, type, and surface chemistry can be

Table 3 Apparent flow rates for different channel widths

Channel width (mm)	Pore radius (μm)	V_{free} (μL)	v_c ($\mu\text{L min}^{-1}$)
1	14.9	3.2	2.3 ± 0.23 – 0.4 ± 0.04
2	14.9	6.4	8.6 ± 0.86 – 1.4 ± 0.14
3	14.9	9.6	11.6 ± 1.15 – 2.4 ± 0.24
4	14.9	12.8	15.5 ± 1.54 – 2.4 ± 0.25
5	14.9	16.0	15.5 ± 1.59 – 2.4 ± 0.25

Table 4 Properties of the cotton linters-based paper substrates

Free pore volume (μL)	Pore radius (μm)	Grammage (g m^{-2})	Thickness (μm)	Porosity
12.8	14.9	23	80	0.80
16.3	8.4	45	110	0.74
22.3	4.3	76	160	0.69
36.5	3.1	161	290	0.63

excluded. Table 4 summarizes the properties of the prepared cotton linters-based paper substrates. Channel widths of the prepared microfluidic papers were maintained at 4 mm to avoid artifacts from the dead-end pores as outlined above.

Capillary-driven fluid transport of an aqueous solution through the paper-defined channels was investigated, as described earlier. Figure 6 illustrates the relationship between the distance travelled by the fluid front inside the channel, as defined by x , as a function of t and $t^{0.5}$. Likewise, a Washburn-type viscous flow was observed for all investigated papers. Depending on the porosity of individual substrates, significant differences in the slope of the studied microfluidic papers were observed (Fig. 6b). A slope of $m \approx 4$ was obtained for paper sheets featuring a mean pore radius of $\sim 15 \mu\text{m}$, whereas a slope of $m \approx 1$ was obtained for paper substrates featuring a mean pore radius of $\sim 3 \mu\text{m}$. The latter result is consistent with the Lucas–Washburn model as described in Eq. 2. Considering absolute time scales, travelling times of the fluid along the straight part of the channel are ~ 3 min (in case of the lab-engineered cotton linters paper sheet with a mean pore radius of $\sim 15 \mu\text{m}$); ~ 7 min (for the paper substrate with a mean pore radius of about $8 \mu\text{m}$); ~ 16 min 30 s (for the paper substrate with a mean pore radius of $\sim 4 \mu\text{m}$); and ~ 27 min 45 s (for the paper substrate with a mean pore radius of about $3 \mu\text{m}$).

Thus, engineering of paper substrates with tailorable porosities allows control and modulation of the kinetics profiles of an aqueous solution through paper-defined channels on an absolute time scale by a factor of ~ 10 . To further understand this phenomenon, average flow rates (Table 5) were calculated as described earlier according to Eq. 3.

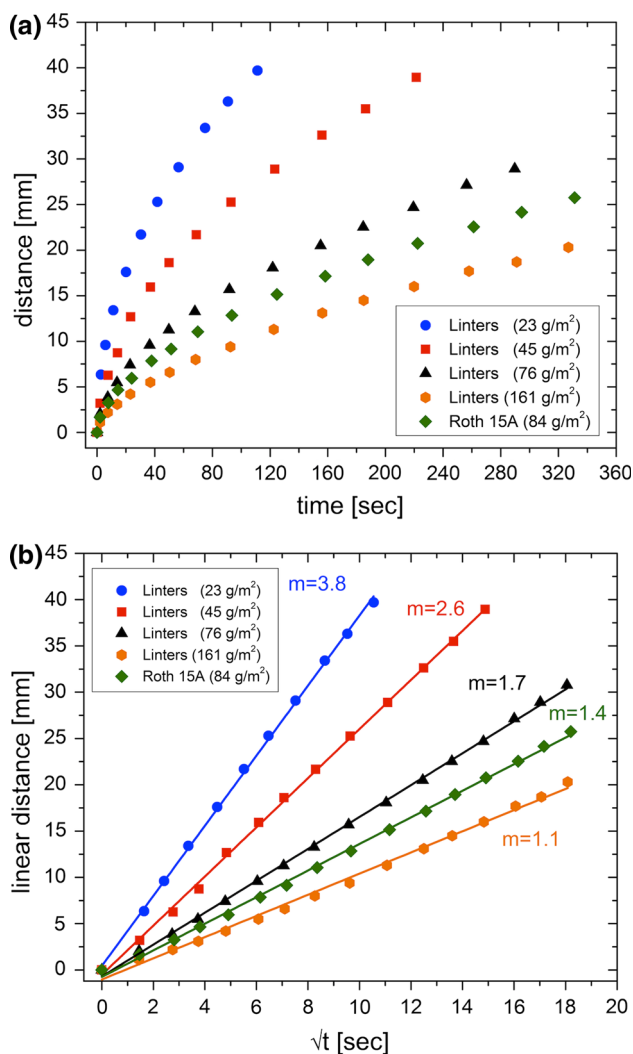


Fig. 6 **a** Comparison of the position, x , of the fluid front driven by capillary action along the channel as a function of $t^{0.5}$ for various cotton linters-based paper substrates with different fiber densities, pore sizes, and free pore volumes, and model filter paper (Roth 15A). Individual data points were captured by video streaming the capillary transport of the fluid inside the channel. A change in the fiber density of the paper substrates (effectively translating to a change in pore size, porosity, and free pore volume of the paper sheets) leads to a significant change in the distance covered by the fluid front within a given time interval. **b** Comparison of the position, x , of the fluid front driven by capillary action along the channel as a function of $t^{0.5}$ for various cotton linters-based paper substrates with different fiber densities, pore sizes, and free pore volumes, and model filter paper (Roth 15A)

Depending on the average pore radius of the paper substrates, the average flow rates near the channel inlet differ over a wide range from $\sim 3.4 \mu\text{L min}^{-1}$ (161 g m^{-2}) up to $\sim 15.5 \mu\text{L min}^{-1}$ (23 g m^{-2}), and those near the channel outlet, vary between $\sim 0.8 \mu\text{L min}^{-1}$ (161 g m^{-2}) and $2.4 \mu\text{L min}^{-1}$ (23 g m^{-2}). The findings demonstrate that by adjusting the porosity and hence the free pore volume of the lab-sheets, fluid transport inside the

Table 5 Apparent flow rates for different linters-based paper substrates

Paper substrate (grammage) (g m^{-2})	Pore radius (μm)	V_{free} (μL)	v_c ($\mu\text{L min}^{-1}$)
Linters 23	14.9	12.8	15.5 ± 1.54 – 2.4 ± 0.25
Linters 45	8.4	16.3	5.9 ± 0.59 – 1.4 ± 0.14
Linters 76	4.3	22.4	3.7 ± 0.36 – 0.8 ± 0.07
Linters 161	3.1	36.5	3.4 ± 0.34 – 0.8 ± 0.08

paper-defined channels can be conveniently controlled in a reproducible fashion over a wide range.

4 Conclusions

In the present study, we demonstrate a novel approach to control and modulate fluid transport inside paper-defined channels by using different customizable lab-engineered paper sheets. We investigated the influence of the fiber source and paper porosities on the capillary-driven fluid transport of aqueous solutions. Lab-engineered paper sheets and commercially available filter papers were investigated for comparative studies. The findings showed that it is difficult to accurately control fluid transport kinetics in the commercially available filter papers. This was attributed to the intrinsic presence of chemical additives in the commercial filter papers that can influence and further complicate fluid transport behaviors. In contrast, lab-engineered papers afford control over the composition of the paper, in particular porosity of the sheets, and it avoids potential side effects from chemical paper additives.

Investigation of the fluid transport in paper channels of varying widths revealed reduced flow rates when the channel is defined by hydrophobic barriers, and the width of the paper channel is smaller than the length of the cellulose microfibers, used during paper sheet fabrication. This observation indicates that knowledge of the length of isotropically distributed fibers in the sheet is essential to achieve regulated fluid transport in microfluidic papers. Varying the fiber orientation could potentially lead to different findings; investigations are currently underway.

Our studies also showed that mean flow rates of an aqueous solution driven by capillary forces through a paper-defined channel can be varied by changing the “packing density” of the cotton linter fibers inside hand-made sheets. The latter yields paper sheets with varying average pore sizes. The mean flow rates varied from ~ 1 to $>15 \mu\text{L min}^{-1}$ when the mean pore radius changed from ~ 3 to $\sim 15 \mu\text{m}$, respectively. It should be noted that the obtained values would change accordingly with time as all

papers featured a Washburn-type viscous flow profile whereby the fluid flow inside the channel follows a $t^{1/2}$ dependency. This property will be important if such microfluidic papers are further considered, e.g., for low-cost, sustainable micro-reactors.

Acknowledgments We thank Martina Ewald and Heike Herbert for various technical support. A. Böhm likes to thank the Excellency cluster “Center of Smart Interfaces, CSI” for a research scholarship. Financial support by the Hessian excellence initiative LOEWE within the cluster SOFT CONTROL and from the Verband der Papierfabriken (VDP), Grant No. INFOR 137, is gratefully acknowledged.

References

- Berchtold B (2005) Oberflächengebundene Polymernetzwerke zur Re-Endothelialisierung von porcinen Herzklappenbioprothesen. Dissertation, Albert-Ludwigs-Universität Freiburg im Breisgau
- Böhm A, Gattermayer M, Trieb C, Schabel S, Fiedler D, Miletzky F, Biesalski M (2013a) Photo-attaching functional polymers onto cellulose fibers for the design of chemically modified paper. *Cellulose* 20(1):467–483
- Böhm A, Gattermayer M, Carstens F, Schabel S, Biesalski M (2013b) Designing microfabricated paper devices through tailored polymer attachment. *Adv Pulp Paper Sci Res*, In: I’Anson SJ (ed) *Trans. XVth fundamental res. symposium*, Cambridge, FRC Cambridge, UK: 599–618
- Brody JP, Yager P, Goldstein RE, Austin RH (1996) Biotechnology at low Reynolds numbers. *Biophys J* 71:3430–3441
- Bruzewicz DA, Reches M, Whitesides GM (2008) Low-cost printing of poly(dimethylsiloxane) barriers to define microchannels in paper. *Anal Chem* 80:3387–3392
- Carrilho E, Martinez AW, Whitesides GM (2009) Understanding wax printing: a simple micropatterning process for paper-based microfluidics. *Anal Chem* 81:7091–7095
- Cheng CM, Martinez AW, Gong J, Mace CR, Phillips ST, Carrilho E, Mirica KA, Whitesides M (2010) Paper-based ELISA. *Angew Chem Int Ed* 49:4771–4774
- Freidank D (2005) 3D-DNA-Chips: oberflächengebundene funktionelle Polymernetzwerke als Matrix für Nukleinsäure-Microarrays. Dissertation, Albert-Ludwigs-Universität Freiburg im Breisgau
- Fu E, Ramsey SA, Kaufmann P, Lutz B, Yager P (2010a) Transport in two-dimensional paper networks. *Microfluid Nanofluid* 10:29–35
- Fu E, Lutz B, Kaufmann B, Yager P (2010b) Controlled reagent transport in disposable 2D paper networks. *Lab Chip* 10:918–920
- Hodgson K, Berg J (1988) The effect of surfactants on wicking flow in fiber networks. *J Colloid Interface Sci* 121:22–31
- Kauffman P, Fu E, Lutz B, Yager P (2010) Visualization and measurement of flow in two-dimensional paper networks. *Lab Chip* 10:2614–2617
- Klasner S, Price A, Hoeman K, Wilson R, Bell K, Culbertson C (2010) Paper-based microfluidic devices for analysis of clinically relevant analytes present in urine and saliva. *Anal Bioanal Chem* 397:1821–1829
- Leung V, Shehata AAM, Filipe CDM, Pelton R (2010) Streaming potential sensing in paper-based microfluidic channels. *Colloids Surf A* 364:16–18
- Li X, Tian J, Nguyen T, Shen W (2008) Paper-based microfluidic devices by plasma treatment. *Anal Chem* 80:9131–9134
- Li X, Tian J, Shen W (2010) Progress in patterned paper sizing for fabrication of paper-based microfluidic sensors. *Cellulose* 17:649–659
- Li X, Ballerini DR, Shen W (2012) A perspective on paper-based microfluidics: current status and future trends. *Biomicrofluidics* 6:011301
- Liana DD, Raguse B, Gooding JJ, Chow E (2012) Recent advances in paper-based sensors. *Sensors* 12:11505–11526
- Lu Y, Shi W, Jiang L, Qin J, Lin B (2009) Rapid prototyping of paper-based microfluidics with wax for low-cost, portable bioassay. *Electrophoresis* 30:1497–1500
- Lucas R (1918) Über das Zeitgesetz des Kapillaren Aufstiegs von Flüssigkeiten. *Colloid Polym Sci* 23:15–22
- Martinez AW, Phillips ST, Butte MJ, Whitesides GM (2007) Patterned paper as a platform for inexpensive, low-volume, portable bioassays. *Angew Chem Int Ed* 46:1318–1320
- Martinez AW, Phillips ST, Whitesides GM (2008) Three-dimensional microfluidic devices fabricated in layered paper and tape. *Proc Natl Acad Sci USA* 105:19606–19611
- Martinez AW, Phillips ST, Whitesides GM (2010) Diagnostics for the developing world: microfluidic paper-based analytical devices. *Anal Chem* 82:3–10
- Noh H, Phillips ST (2010a) Metering the capillary-driven flow of fluids in paper-based microfluidic devices. *Anal Chem* 82:4181–4187
- Noh H, Phillips ST (2010b) Fluidic “timers” for paper-based microfluidic devices. *Anal Chem* 82:8071–8078
- Osborn JL, Lutz B, Fu E, Kauffmann P, Stevens DY, Yager P (2010) Microfluidics without pumps: reinventing the T-sensor and H-filter. *Lab Chip* 10:2659–2665
- Phillips ST, Lewis GG (2013) Advances in materials that enable quantitative point-of-care assays. *MRS Bull* 38:315–319
- Prucell EM (1977) Life at low Reynolds-numbers. *Am J Phys* 45:3–11
- Songjaroen T, Dunchai W, Chailapakul O, Henry CS, Laiwattanapaisal W (2012) Blood separation on microfluidic paper-based analytical devices. *Lab Chip* 12:3392–3398
- Washburn EW (1921) The dynamics of capillary flow. *Phys Rev* 17:273–283